AD-A159 500 A NEW CORRECTION TO SCHOTTKY BARRIER LOWERING IN CATHODES(U) AEROSPACE CORP EL SEGUNDO CA CHEMISTRY AND PHYSICS LAB G ENG 15 JUL 85 TR-0084A(5945-02)-1 1/1

UNCLASSIFIED SD-TR-85-42 F04701-83-C-0084 F/G 9/1 NL

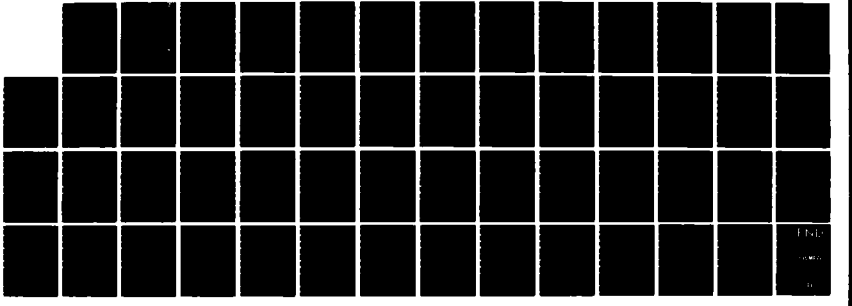

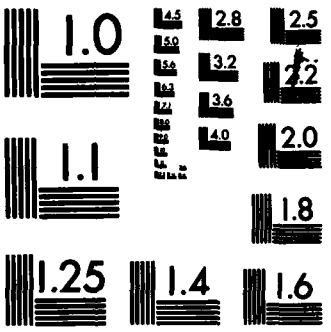

MICROCOPY RESOLUTION TEST CHART
NATIONAL BUREAU OF STANDARDS-1963-A

REPORT NO. SD-TR-85-42

A New Correction to Schottky Barrier Lowering in Cathodes

G. ENG
Chemistry and Physics Laboratory
Laboratory Operations
The Aerospace Corporation
El Segundo, CA 90245

15 July 1985

Prepared for

SPACE DIVISION
AIR FORCE SYSTEMS COMMAND
Los Angeles Air Force Station
P.O. Box 92960, Worldway Postal Center
Los Angeles, CA 90009-2960

This report was submitted by The Aerospace Corporation, El Segundo, CA 90245, under Contract No. F04701-83-C-0084 with the Space Division, P.O. Box 92960, Worldway Postal Center, Los Angeles, CA 90009-2960. It was reviewed and approved for The Aerospace Corporation by S. Feuerstein, Director, Chemistry and Physics Laboratory. Lt. Charles C. Neidhardt, SD/CGX, was the project officer for the Mission-Oriented Investigation and Experimentation (MOIE) Program.

This report has been reviewed by the Public Affairs Office (PAS) and is releasable to the National Technical Information Service (NTIS). At NTIS, it will be available to the general public, including foreign nationals.

This technical report has been reviewed and is approved for publication. Publication of this report does not constitute Air Force approval of the report's findings or conclusions. It is published only for the exchange and stimulation of ideas.

Charles C Neidhart

CHARLES C. NEIDHART, Lt, USAF
MOIE Project Officer
SD/CGX

Joseph Hess

JOSEPH HESS, GM-15
Director, AFSTC West Coast Office
AFSTC/WCO OL-AB

UNCLASSIFIED

SECURITY CLASSIFICATION OF THIS PAGE (When Data Entered)

REPORT DOCUMENTATION PAGE		READ INSTRUCTIONS BEFORE COMPLETING FORM
1. REPORT NUMBER SD-TR-85-42	2. GOVT ACCESSION NO. AD-A159 500	3. RECIPIENT'S CATALOG NUMBER
4. TITLE (and Subtitle) A New Correction to Schottky Barrier Lowering in Cathodes		5. TYPE OF REPORT & PERIOD COVERED
		6. PERFORMING ORG. REPORT NUMBER TR-0084A(5945-02)-1
7. AUTHOR(s) Genghmun Eng		8. CONTRACT OR GRANT NUMBER(s) F04701-83-C-0084
9. PERFORMING ORGANIZATION NAME AND ADDRESS The Aerospace Corporation El Segundo, Calif. 90245		10. PROGRAM ELEMENT, PROJECT, TASK AREA & WORK UNIT NUMBERS
11. CONTROLLING OFFICE NAME AND ADDRESS Space Division Los Angeles Air Force Station Los Angeles, Calif. 90009-2960		12. REPORT DATE 15 July 1985
		13. NUMBER OF PAGES 46
14. MONITORING AGENCY NAME & ADDRESS(if different from Controlling Office)		15. SECURITY CLASS. (of this report) Unclassified
		15a. DECLASSIFICATION/DOWNGRADING SCHEDULE

16. DISTRIBUTION STATEMENT (of this Report)

Approved for public release; distribution unlimited.

17. DISTRIBUTION STATEMENT (of the abstract entered in Block 20, if different from Report)

18. SUPPLEMENTARY NOTES

19. KEY WORDS (Continue on reverse side if necessary and identify by block number)

Thermionic Emission
Electron Emission
Electron Beams
Space-Charge Effects
Cathodes
Schottky Barrier
Cathode Emission

20. ABSTRACT (Continue on reverse side if necessary and identify by block number)

A new technique is developed for approximating cathode current-voltage (I-V) and current-temperature (I-T) characteristics in a planar diode configuration. For a uniform work function surface, this method allows both for space-charge effects and for Schottky barrier lowering. Using this method, we derive an explicit first correction to the Schottky effect:

$$\Delta\phi_{new} = \Delta\phi_o \left(1 - \frac{J_{net}}{J_C}\right)^{1/2},$$

DD FORM 1473 (FACSIMILE)

UNCLASSIFIED

SECURITY CLASSIFICATION OF THIS PAGE (When Data Entered)

19. KEY WORDS (Continued)

20. ABSTRACT (Continued)

where $\Delta\phi_o$ is the standard Schottky barrier lowering (eV), J_{net} is the net emission current density, and J_C is the Child's Law current density. The following closed form expression then approximates the net emission current density:

$$J_{net} = J_C, \ (J_R > J_C), \text{ and}$$

$$J_{net} = J_R \exp\left(\Delta\phi_{new}/kT\right), \ (J_R < J_C),$$

where J_R is the Richardson's current density. This equation for J_{net} connects the space-charge limited (SCL) emission regime to the deep temperature-limited (TL) regime. The SCL-to-TL transition point is found to be J_R, and the emission current, above, is continuous with a continuous slope at the transition point.

PREFACE

The author is deeply indebted to Dr. T. P. Lin, Professor of Mathematics, California State University at Northridge, for the early access to his exact numerical calculation results, prior to their publication, and for his help in aiding the successful completion of this work. Special thanks also is due to Capt. J. B. Scott who gave us a copy of his program for calculating I-V curves, which was used to generate part of Section IV. The author also thanks Dr. H. K. A. Kan for his support and advice.

CONTENTS

FIGURES

I. INTRODUCTION

Understanding cathode behavior is one of the most crucial areas confronting manufacturers of travelling wave tube (TWT) amplifiers. The need for long lifetime, high emission current, and high reliability for potential space applications means that more stringent testing and evaluation procedures are needed to help select suitable devices. Here we address one such crucial area, that of the expected cathode emission current. The net emission current under given specific conditions is the single most used criterion for evaluating cathode performance. Until recently, full understanding of the cathode I-V and I-T characteristics for even a uniform work function surface was not yet developed. Expressions were known in the limit of low applied voltage or high temperature, and in the limit of high applied voltage or low operating temperature.

A full solution to the uniform work function planar diode requires both the effects of space-charge and Schottky barrier-lowering to be included, if one is to cover the entire spectrum from space-charge limited (SCL) to temperature-limited (TL) emission. Our work builds on the historical work of Richardson,[1] Dushman,[2] Child,[3] Langmuir,[4] and Schottky,[5] and it addresses the problem of extending and combining the Langmuir-Child (SCL) currents with the Richardson-Schottky (TL) currents. It is similar in spirit to the work of Nottingham,[6] Van der Zeil,[7] Crowell,[8] Rittner,[9] and, recently, Longo[10] Scott[11], and Hasker.[12]

We use the same basic derivation method as Langmuir[4] for the space-charge effects, but we outline a new technique for approximating the solution to the difficult equations when Schottky barrier lowering is added. Here, an approximate potential is used to help decouple the nonlinearity of Poisson's equation, which arises due to space-charge effects. We call this method an "effective potential" approximation, since it replaces the true potential with an "effective" potential in one step of the calculation.

The effective potential approximation sacrifices the exactness of a numerical solution in order to gain an easier applicability to understanding

emission data. In addition, an approximate analytical answer can be used to help make the underlying physical processes affecting the emission current more transparent, and to qualitatively predict trends as a particular parameter is varied.

In Sec. II of this report, we outline some of the physical assumptions made in the present solution. In Sec. III we construct the approximate solution to the nonlinear Poisson's equation. Here particular attention is given to how the boundary conditions should be handled. Indeed, much of the simplicity of our final answer results from carefully preserving both the boundary conditions and conserved parameters.

In Sec. IV, the case of the uniform work function surface is considered in detail, using this method. We analyze how the present technique reproduces the Child's Law current at low applied fields, and how it converges to the Schottky barrier-lowering effect in very high applied fields.

The major result of this report is then derived. A simple closed form solution is presented for approximating the net emission current, which goes smoothly from space-charge limited (SCL) to temperature-limited (TL) operation. This new solution primarily corrects the Schottky barrier lowering effect, to include the persistence of space-charge effects, even at high fields. This result also shows that the SCL-to-TL transition point is the Richardson's current, and it specifies the "roundedness" of the knee near the SCL-to-TL transition region.

II. THE PHYSICAL BASIS OF CATHODE I-V AND I-T CURVES

A. POISSON'S EQUATION

The effects of a space-charge cloud on cathode current-voltage (I-V) and current-temperature (I-T) characteristics are usually examined by using Poisson's equation:

$$\nabla^2 V = -\rho/\varepsilon_o. \tag{1}$$

This equation relates the local net charge density, ρ, in the space-charge cloud, to the electrostatic potential, V, where ε_o is the permittivity of free space. The electrostatic potential can be converted to electrostatic potential energy, θ_i, by $\theta_i = q_i V$, where q_i is the charge of the particle under the influence of V. Also, $\rho(\vec{r})$ for the surrounding medium can be written as:

$$\rho(\vec{r}) = q_j \tilde{n}(\vec{r}), \tag{2}$$

where $\tilde{n}(\vec{r})$ is the positive number density of particles in the medium, and q_j is their individual charge. For electrons interacting with an electron space-charge cloud, Poisson's equation becomes:

$$\nabla^2\theta(\vec{r}) = -e^2 \tilde{n}(\vec{r})/\varepsilon_o, \tag{3}$$

where $e = +1.602 \times 10^{-19}$ coulombs.

When image force effects are included, $\tilde{n}(\vec{r})$ will contain both a bulk term $n(\vec{r})$, describing the average properties of the space-charge cloud, and a singular term $\delta(\vec{r})$, which is a Dirac delta-function term describing the electrode reaction to an individual discrete electron.

An equivalent formulation is to first solve Poisson's equation in the zero current case for θ_{ext}, where:

$$\nabla^2\theta_{ext}(\vec{r}) = +e\,\rho_{ext}(\vec{r})/\varepsilon_o, \tag{4}$$

and where $\rho_{ext}(\vec{r})$ contains all the singular aspects of the charge distribution. The monopole contribution to $\rho_{ext}(\vec{r})$ is due to image forces on an individual electron, and to charges on the plates from placing an external applied voltage between the electrodes. The dipole contribution to $\rho_{ext}(\vec{r})$ is due to the surface work function (ϕ), or work function distribution on the electrodes.

When there is a net current flow between the plates, one can then solve:

$$\nabla^2 [\theta(\vec{r}) - \theta_{ext}(\vec{r})] = -e^2 n(\vec{r})/\varepsilon_o, \tag{5}$$

where $\theta(\vec{r})$ is the total electron potential energy at any point $\vec{r}$ between the electrodes, and $n(\vec{r})$ is the local bulk space-charge density at that point, which is non-singular. Using the $\theta_{ext}(\vec{r})$ function assures convergence to the proper solution when the bulk space-charge density $n(\vec{r})$ vanishes. The $n(\vec{r})$ bulk charge density would vanish, for example, when the cathode temperature is lowered under constant applied field conditions, as in a dip test.

We next simplify the problem to one rectilinear dimension, x, which is the planar diode configuration, resulting in:

$$\frac{d^2}{dx^2} [\theta(x) - \theta_{ext}(x)] = -e^2 n(x)/\varepsilon_o. \tag{6}$$

Often, there is only one direction of interest, defined by the average net current flow direction, but in many applications the electrodes may contain curved surfaces. However, since much of the net current determination involves what happens within microns of the cathode surface, using an "effective distance" parameter in Eq. (6) may help the planar diode solution to be applied to these curved geometries.

B. APPROXIMATIONS USED IN DERIVING THE SOLUTION

What makes the solution to Eq. (6) difficult is that the local charge density between the plates, n(x), is determined by the amount of current flowing, which in turn is determined by various aspects of the $\theta(x)$ curve

itself. This effect changes $n(x)$ into $n(\theta(x))$, making Eq. (6) inherently nonlinear. In the effective potential approximation technique, this nonlinearity is circumvented by replacing the $\theta(x)$ function in the $n(\theta(x))$ term with an effective potential function which retains the most important characteristics of the true $\theta(x)$ function. This technique is much like replacing a known non-elementary function by a polynominal fit to that function.

A second difficulty in Eq. (6) is that the $\theta(x)$ function necessarily has a maximum in it, at some point x_c between the electrode plates. The maximum point in $\theta(x)$, denoted

$$\max\ [\theta(x)] \equiv \theta(x_c) \equiv E_c, \tag{7}$$

then represents a potential energy barrier which electrons must overcome in order to be registered as collected current. Electrons emitted with an energy lower than this barrier height E_c will be reflected back into the cathode. The reflected electrons do not contribute to the collected current, but they can alter the local $n(x)$ net electron density, forming a "trapped cloud" in the near cathode region.

In much of this work, we neglect the contribution to $n(x)$ due to electrons in the trapped cloud. It is equivalent to assuming that only electrons with enough energy to surmount the barrier are emitted. We shall see later that at low voltages the present calculation for x_c and E_c can give x_c values which can be a significant fraction of the total anode-to-cathode distance d. Such a wide extent for the barrier position means that if the calculation included the effect of a few electrons forming a trapped cloud with energies near E_c, they would not change the barrier height by much. However, by interacting among themselves, they could alter the barrier position significantly. Thus, by neglecting these electrons forming a trapped cloud, we expect to overestimate the barrier position x_c by a fair margin, especially in the space-charge limited region, but the net barrier height E_c may not be affected as much.

III. CONSTRUCTION OF THE APPROXIMATE SOLUTION

A. THE ELECTRON DENSITY IN THE SPACE-CHARGE CLOUD

Figure 1 shows the potential energy diagram for electrons between the two electrodes. The zero of potential energy, E=0, is referenced to the vacuum level, i.e., the potential energy at large distances, extrapolated to zero net field between the electrodes. The x=0 point is the cathode emitter plate, and x=d is the anode collector plate. The net barrier height and the barrier position are labelled E_c and x_c, respectively. We next develop the approximation techniques to estimate both E_c and x_c, given a set of conditions, such as emitter work function ϕ_e, temperature T, applied voltage V_A, and anode-cathode distance d.

Poisson's equation [Eq. (6)], must be solved in the presence of two conserved quantities:

a) Conserved total electron energy:

$$\frac{1}{2}\, m\, v(x)^2 + \theta(x) = E, \tag{8a}$$

$$v(x,E) = \left\{2[E-\theta(x)]/m\right\}^{1/2},\ E > \theta\ (x). \tag{8b}$$

b) Conserved forward current, independent of position:

$$dJ_+ = (A_o/k)\ T \exp\ [-(E+\phi_e)/kT]\ dE, \tag{9a}$$

$$A_o = \frac{4\pi mek^2}{h^3} \equiv 119.58\ \text{amps}/(\text{cm}^2\ \text{K}^2), \tag{9b}$$

where A_o is Richardson's constant and k is Boltzmann's constant. The net current is derived from Eq. (9a) by summing all the current contributions from $E = (E_c, \infty)$.

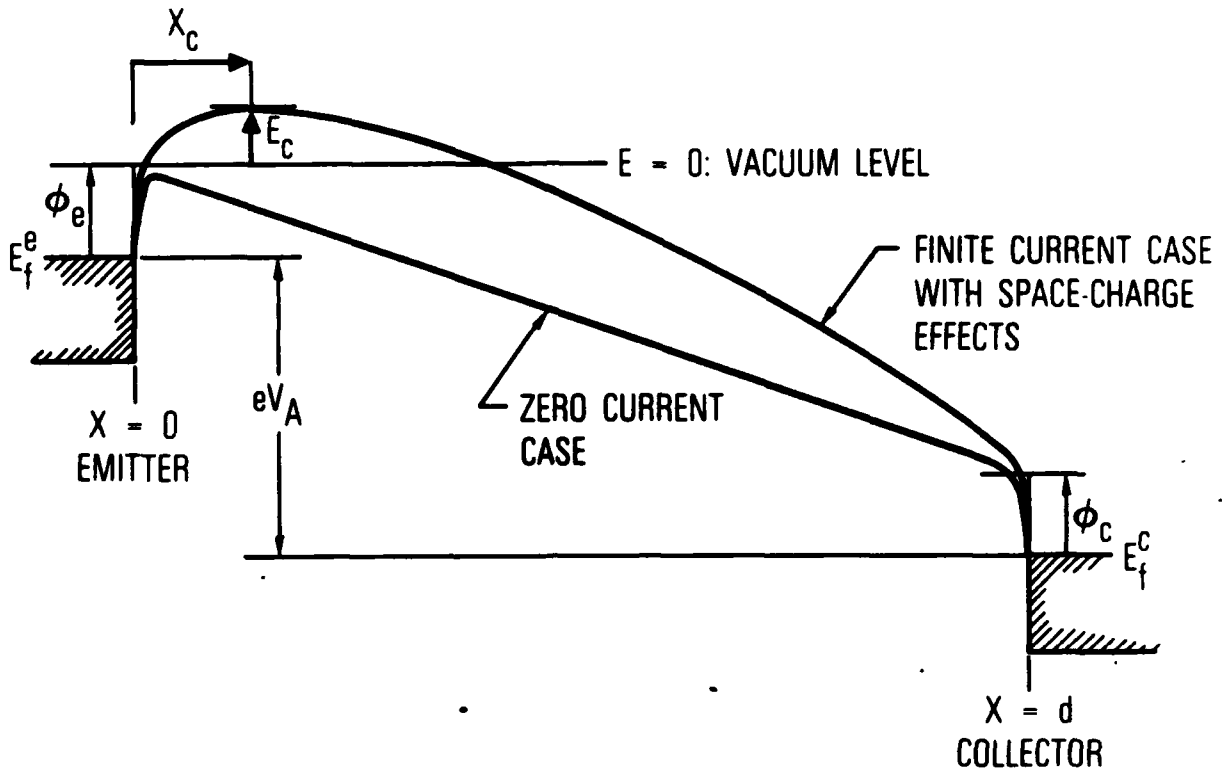

Fig. 1: Schematic of the inter-electrode potential energy vs. distance, zero-current, and finite current cases. The emitter and collector work functions (ϕ_e and ϕ_c) and their Fermi levels (E_f^e, E_f^c) are shown, along with the applied voltage V_A. The space-charge associated with a finite emitter-to-collector current causes an electron barrier to develop, denoted E_c, which can be several microns away from the cathode, at a position labelled x_c. Only electrons emitted with energies greater than E_c are collected as the emitted current density.

In Poisson's equation, the local number density of electrons n(x) can be written as:

$$n(x) = \int_{(\text{all } E)} n(x,E) \quad dE. \tag{10}$$

The n(x,E) term includes all electrons with an energy greater than E_c, which become part of the collected current, as well as those electrons with energies less than E_c, which could form a trapped cloud near the emitter. Neglecting the contribution to n(x) due to electrons with energies $E < E_c$ constitutes the "empty cloud" approximation used here. Equation (10) then becomes:

$$n(x) \approx \int_{E=E_c}^{\infty} n\,(x,E) \quad dE, \tag{11a}$$

$$n\,(x,E)\,dE = \frac{n\,(x,E)\;e\;v(x,E)\;\;dE}{e\;v(x,E)} = \frac{dJ_+}{e\;v\;(x,E)}\,. \tag{11b}$$

Direct substitution of Eqs. (8) and (9) into Eqs. (11a)-(11b) yields:

$$n(x) \approx \left(\frac{\pi}{4}\right)^{1/2} \left(\frac{2A_o\,T^2}{ec}\right) \left(\frac{mc^2}{2kT}\right)^{1/2} f(y_c^{\,2})\, \exp\,[-(E_c + \phi_e)kT], \tag{12a}$$

$$f(y_c^{\,2}) \equiv (4/\pi)^{1/2} \exp\,(+\,y_c^{\,2}) \int_{y=y_c}^{\infty} dy\, \exp\,(-y^2) \tag{12b}$$

$$= \exp\,(+\,y_c^{\,2})\, \text{erfc}\,(y_c),$$

$$y_c^{\,2}(x) \equiv [E_c - \theta(x)]/kT. \tag{12c}$$

Defining:

$$n_o = \left[\frac{A_o\,T^2}{ec}\right] \left[\frac{\pi\;mc^2}{2\;kT}\right]^{1/2} \exp\,[-(E_c+\phi_e)/kT], \tag{13}$$

it then corresponds to the density of electrons at the barrier maximum, with c being the speed of light. Equation (13) also shows that this electron density is proportional to the net collected current. Poisson's equation, using Eq. (11a), then becomes:

$$\frac{d^2}{dx^2}\,[\theta(x) - \theta_{ext}(x)] = \frac{-e^2 n_o}{\epsilon_o}\; f[y_c^{\,2}(x)]. \tag{14}$$

The approximate solution to this equation is developed next.

B. SOLUTION TO POISSON'S EQUATION AND BOUNDARY CONDITIONS

The solution to Eq. (14) can be formally be written as:

$$\theta(x) - \theta_{ext}(x) = K_o x + B_o - \frac{e^2 n_o}{\epsilon_o} \int_{x_1=0}^{x} dx_1 \int_{x_2=0}^{x_1} dx_2 \;\; f[y_c^{\,2}(x_2)], \tag{15}$$

where K_o and B_o are constants. The double integral can be transformed into a single integral[13]:

$$\theta(x) - \theta_{ext}(x) = K_o x + B_o - \frac{e^2 n_o}{\epsilon_o} \int_{z=0}^{x} (x-z)\, dz \;\; f(y_c^{\,2}(z)). \tag{16}$$

The $K_o x$ and B_o terms in Eq. (16) give the electrode reaction to the presence of the space-charge cloud between the plates.

The boundary conditions at the electrode plates are next applied. To preserve $\theta(x=0) = \theta_{ext}(x=0)$, one must set $B_o=0$. To preserve $\theta(x=d) = \theta_{ext}(x=d)$, requires that:

$$K_o d = \frac{e^2 n_o}{\epsilon_o} \int_{z=0}^{d} (d-z)\, dz\; f[y_c^{\,2}(z)], \tag{17}$$

determining the value for K_o.

Next, define two helping functions:

$$g(x) = \int_{z=0}^{x} f[y_c^2(z)]\, dz, \tag{18a}$$

$$h(x) = \int_{z=0}^{x} f[y_c^2(z)]\, z\, dz, \tag{18b}$$

and one can derive the following expressions for $\theta(x)$ and $d\theta(x)/dx$:

$$\theta(x) - \theta_{ext}(x) = \frac{+e^2 n_o}{\varepsilon_o d} \{x\, d\, [g(d)-g(x)] + h(x)\, d - h(d)\, x\}, \tag{19a}$$

$$\frac{d\theta(x)}{dx} - \frac{d\theta_{ext}(x)}{dx} = \frac{+e^2 n_o}{\varepsilon_o d} \{d\, [g(d) - g(x)] - h(d)\}. \tag{19b}$$

From these two equations, two other combinations can be constructed. The first combination is:

$$[\theta(x) - \theta_{ext}(x)] - x \left(\frac{d\theta}{dx} - \frac{d\theta_{ext}}{dx}\right) = \frac{e^2 n_o}{\varepsilon_o} [h(x)], \tag{20}$$

and it involves the nonlinear part of Poisson's equation only in the region between x=0 and the present value of x, through the h(x) function. The second combination is:

$$[\theta(x) - \theta_{ext}(x)] + (d-x) \left(\frac{d\theta}{dx} - \frac{d\theta_{ext}}{dx}\right) =$$

$$\frac{+e^2 n_o}{\varepsilon_o} \{d\, [g(d)-g(x)] - [h(d)-h(x)]\}, \tag{21}$$

and this involves the nonlinear part, through the g(x) and h(x) functions, only in the region between the present value of x and the collector at x=d.

The general shape of $\theta(x)$, as shown in Fig. 1, has a single maximum within the range x=(0,d), occurring at $x = x_c$, with $\max[\theta(x)] \equiv E_c$. Since Eqs. (20) and (21) are valid for all x, it is more convenient to use Eq. (20)

for describing the region of $x=(0,x_c)$, and to use Eq. (21) for describing the region $x = (x_c,d)$. By deriving equations which separate the region $x=(0,x_c)$ from the region $x=(x_c,d)$, one can easily apply the condition which requires $x=x_c$ to correspond to the maximum point in $\theta(x)$.

The separation into $x<x_c$ and $x>x_c$ regions also allows the solution to be expressed in terms of scaled distance variables. It makes the evaluation of expressions in the critical $x \approx x_c$ region easier. We use the following scaled variables:

$$\gamma = x/d, \quad \gamma_o = x_c/d, \tag{22a,b}$$

$$U = (x/x_c) - 1, \tag{22c}$$

$$W = [(x-x_c)/(d-x_c)], \tag{22d}$$

so that $U = (-1, 0)$ when $x = (0, x_c)$, and $W = (0, +1)$ when $x = (x_c,d)$. The terms in Eqs. (20) and (21) involving the nonlinear functions, $g(x)$ and $h(x)$, can then be expressed in terms of the following functions:

$$G_1\left(U = \frac{x}{x_c} - 1\right) = \int_{u=-1}^{U} f[u]\, du, \tag{23a}$$

$$H_1\left(U = \frac{x}{x_c} - 1\right) = \int_{u=-1}^{U} f[u]\, u\, du, \tag{23b}$$

$$G_2\left(W = \frac{x-x_c}{d-x_c}\right) = \int_{w=W}^{1} f[w]\, dw, \tag{23c}$$

$$H_2\left(W = \frac{x-x_c}{d-x_c}\right) = \int_{w=W}^{1} f[w]\, w\, dw, \tag{23d}$$

By using these scaled-variable functions, Eqs. (20) and (21) become:

$$[\theta(x) - \theta_{ext}(x)] - \gamma\, d\left(\frac{d\theta}{dx} - \frac{d\theta_{ext}}{dx}\right)$$

$$= \left(\frac{e^2 n_o d^2}{\varepsilon_o}\right) \gamma_o^2 \left[G_1(U) + H_1(U)\right], \tag{24a}$$

$$[\theta(x) - \theta_{ext}(x)] + (1 - \gamma)\, d\left(\frac{d\theta}{dx} - \frac{d\theta_{ext}}{dx}\right)$$

$$= \left(\frac{e^2 n_o d^2}{\varepsilon_o}\right) (1 - \gamma_o)^2 \left[G_2(W) - H_2(W)\right]. \tag{24b}$$

The last boundary condition can now be easily applied. It requires that at $x = x_c$, both the following conditions must be satisfied:

$$\frac{d\theta(x)}{dx} = 0 \quad (\text{at } x = x_c), \tag{25a}$$

$$\theta(x) = E_c \quad (\text{at } x = x_c). \tag{25b}$$

Applying these conditions to Eqs. (24a) and (24b) then results in the following two algebraic equations, for the two unknowns, E_c, and x_c:

$$[E_c - \theta_{ext}(x_c)] - \gamma_o \left(-d \left.\frac{d\theta_{ext}}{dx}\right|_{x_c}\right)$$

$$= \left(\frac{e^2 n_o d^2}{\varepsilon_o}\right) \gamma_o^2 \left[G_1(0) + H_1(0)\right], \tag{26a}$$

$$[E_c - \theta_{ext}(x_c)] + (1 - \gamma_o) \left(-d \left.\frac{d\theta_{ext}}{dx}\right|_{x_c}\right)$$

$$= \left(\frac{e^2 n_o d^2}{\varepsilon_o}\right) (1 - \gamma_o)^2 \left[G_2(0) - H_2(0)\right]. \tag{26b}$$

This method has manipulated the nonlinear Poisson's equation to emphasize the two parameters of interest: the net barrier height E_c, and the barrier position x_c. It also shows what part of the full solution to the differential equation couples into the E_c and x_c determination. Equations (26a) and (26b) show that the nonlinearities involve only the $[G_1(0) + H_1(0)]$ and $[G_2(0) - H_2(0)]$ terms, both of which are independent of $\gamma_o = x_c/d$. What we have done is to preserve the boundary conditions and symmetries inherent in the original problem, while seeking out E_c and x_c.

C. THE EFFECTIVE POTENTIAL APPROXIMATION

Equations (26a) and (26b) are now in a suitable form for using an effective potential approximation. Since the nonlinear terms (G_1, G_2, H_1,H_2) contain only E_c and integrals over whole portions of the $\theta(x)$ function, the evaluation of $G_1(0)$, $H_1(0)$, $G_2(0)$, and $H_2(0)$ in Eqs. (26a) and (26b) is less sensitive to the exact details of the $\theta(x)$ function than if these terms contained terms involving $\theta(x)$ directly or derivatives of $\theta(x)$. The potential energy curve $\theta(x)$ enters into the nonlinear terms through the definition of y_c:

$$y_c^2(z) = [E_c - \theta(z)]/kT, \tag{27}$$

where z is the integrand variable in each non-linear function.

To evaluate the nonlinear terms in Eqs. (23a)-(23d), we approximate the true $\theta(z)$ function in these integrals by a polynomial in z, or by a power-law function in z. This replacement of the true $\theta(z)$, which is a difficult transcendental function, by an approximating elementary function, is equivalent to substituting an effective potential in for $\theta(x)$. The choices available for the effective potential function can be narrowed by requiring the function to obey known critical properties of the true $\theta(z)$ function.

For the region $x = (0, x_c)$ three boundary conditions on $\theta(x)$ must be satisfied by the effective potential:

$$\theta(x=0) = -\phi_e, \tag{28a}$$

$$\theta(x=x_c) = E_c, \tag{28b}$$

$$\left.\frac{d\theta(x)}{dx}\right|_{x_c} = 0. \tag{28c}$$

The simplest polynominal function in x, which obeys these three conditions, is the parabola:

$$\theta(x) = -(\phi_e + E_c)\,[1 - (x/x_c)]^2 + E_c. \tag{29}$$

The parabola is also special, because it corresponds to an approximately uniform net charge density near the cathode, making the near-cathode region much like a "virtual cathode" from which emission current can be drawn. This parabolic approximation then gives:

$$y_c^2(z) = [1 - (z/x_c)]^2\,(\phi_c + E_c)/kT. \tag{30a}$$

$$y_c^2[u] = u^2\,(\phi_e + E_c)/kT \tag{30b}$$

Equation (30b) can then be substituted into the G_1 and H_1 integrals [Eqs. (23a)-(23b)].

For the region $x = (x_c,d)$, the following boundary conditions need to be satisfied by the effective potential:

$$\theta(x=x_c) = E_c, \tag{31a}$$

$$\left.\frac{d\theta(x)}{dx}\right|_{x_c} = 0, \tag{31b}$$

$$\theta(x=d) \equiv -\theta_E = -(eV_A + \phi_e - \phi_c), \tag{31c}$$

where V_A is the applied external voltage, and ϕ_c is the collector or anode work function. Here, we could also use a polynomial to approximate the $\theta(x)$ function for the $x = (x_c,d)$ region. However, an additional piece of information is available from Child's Law, which says that for large x, away from the emitter:

$$\theta(x) \approx (\text{const.})\ x^{4/3}. \tag{32}$$

We thus choose the following, as the simplest effective potential for the $x = (x_c,d)$ region, and one which satisfies Eqs. (31a,b,c) and (32):

$$\theta(x) \approx E_c - (\theta_E + E_c)\ [(x-x_c)/\ (d-x_c)]^{4/3}. \tag{33}$$

This choice then gives:

$$y_c^{\,2}(z) = [(z-x_c)/(d-x_c)]^{4/3}\ (\theta_E + E_c)/kT, \tag{34a}$$

$$y_c^{\,2}[w] = w^{4/3}\ (\theta_E + E_c)/kT. \tag{34b}$$

Equation (34b) can then be substituted into the G_2 and H_2 integrals [Eqs. (23c)-(23d)].

Grouping the nonlinear terms together in the main equations [Eqs. (26a)-(26b)], and defining new functions, f_k and f_y:

$$f_k \equiv [G_1(0) + H_1(0)], \tag{35a}$$

$$f_y \equiv [G_2(0) - H_2(0)], \tag{35b}$$

gives the following for the function f_k:

$$f_k[\Lambda = (\phi_e + E_c)/kT] = \int_{u=1}^{0} (1+u)\ du\ f(y_c^2 = \Lambda u^2), \tag{36}$$

and it gives for f_y:

$$f_y[\Lambda = (\theta_E + E_c)/kT] = \int_{w=0}^{1} (1-w)\, dw\, f(y_c^2 = \Lambda w^{4/3}). \tag{37}$$

Finally, the function $f(y_c^2)$ in the integrand [see Eq. (12b)] can also be approximated by algebraic functions.

Abramowitz and Stegun[14] place bounds on the $f(y_c^2)$ function:

$$\frac{(4/\pi)^{1/2}}{y_c + (y_c^2 + 2)^{1/2}} < f(y_c^2) < \frac{(4/\pi)^{1/2}}{y_c + (y_c^2 + (4/\pi))^{1/2}} \equiv f_o(y_c^2). \tag{38}$$

The upper bound in Eq. (38) at $y_c \equiv 0$ corresponds to the point $\theta(x) = E_c$. We use this upper bound to the $f(y_c^2)$ function, denoted $f_o(y_c^2)$, here because it overestimates both the density of charges and the magnitude of space-charge effects. It compensates in part for not explicitly considering electrons forming a trapped cloud near the cathode [see Eqs. (10)-(11)], which underestimated the space-charge cloud effects.

Using the $f_o(y_c^2)$-function then gives:

$$f_k[\Lambda = (\phi_e + E_c)/kT] = \int_{u=-1}^{0} (1+u)\, du\, \frac{(4/\pi)^{1/2}}{(\Lambda u^2)^{1/2} + [\Lambda u^2 + (4/\pi)]^{1/2}}, \tag{39a}$$

$$f_y[\Lambda = (\theta_E + E_c)/kT] = \int_{w=0}^{1} (1-w)\, dw\, \frac{(4/\pi)^{1/2}}{(\Lambda w^{4/3})^{1/2} + [\Lambda w^{4/3} + (4/\pi)]^{1/2}}, \tag{39b}$$

as explicit integrals for approximating the nonlinear terms in Poisson's equation. These integrals are worked out in the appendix.

D. DETERMINING THE BARRIER HEIGHT AND BARRIER POSITION

In Eqs. (39a) and (39b) both f_y and f_k are functions of the net barrier height E_c, but not of the barrier position x_c. The f_y and f_k functions contain all the effects of the nonlinearity of the original Poisson's equation. In addition, the f_y and f_k functions naturally separate the solution into a cathode work function term, $f_k(E_c, \phi_e)$, and an applied field term, $f_y(E_c, \theta_E)$. If one were to use a different effective potential function than those chosen here [see Eqs. (29) and (33)], the f_y and f_k functions would still be of the general form:

$$f_y(\Lambda) \approx (\text{const.})/\Lambda^{1/2}, \tag{40a}$$

$$f_k(\Lambda) \approx (\text{const.})/\Lambda^{1/2}. \tag{40b}$$

Additional properties of Eqs. (26a) and (26b) can be used to help make the determination of the roots E_c and x_c easier. Using the following definitions:

$$\alpha_o = E_c - \theta_{ext}(x_c), \tag{41a}$$

$$\beta_o(x_c) = -d \left.\frac{d\theta_{ext}}{dx}\right|_{x_c}, \tag{41b}$$

$$m_o = \frac{e^2 d^2}{\varepsilon_o} n_o, \tag{41c}$$

then allows Eqs. (26a) and (26b) to be rewritten as:

$$\beta_o/m_o = [(1-\gamma_o)^2 f_y(E_c) - \gamma_o^2 f_k(E_c)], \tag{42a}$$

$$\alpha_o - \gamma_o\beta_o = m_o \gamma_o^2 f_k(E_c). \tag{42b}$$

The m_o term is a strong function of E_c, and it is independent of position:

$$m_o = m_R \exp\,[-E_c/kT], \tag{43a}$$

$$m_R \equiv \left(\frac{A_o T^2}{ec}\right)\left(\frac{\pi\, mc^2}{2\, kT}\right)^{1/2}\left(\frac{e^2 d^2}{\varepsilon_o}\right)\exp\left(-\phi_e/kT\right). \tag{43b}$$

The α_o term is an implicit function of both x_c and E_c, and it represents the net barrier height increase caused by the presence of the space-charge cloud. For accelerating field conditions ($\theta_E > 0$), β_o is positive, resulting in the following inequality:

$$\frac{(f_y)^{1/2}}{(f_y)^{1/2} + (f_k)^{1/2}} > \gamma_o \equiv \frac{x_c}{d}. \tag{44}$$

This inequality can be used to help narrow the range of possible x-values to regions much smaller than x=(0,d), when seeking the roots of Eqs. (42a) and (42b). Equation (44) also shows how the presence of the space-charge cloud has naturally placed an upper bound on how far x_c can wander away from the cathode.

Solving for m_o and α_o in Eqs. (42a) and (42b), then gives:

$$\ell n\left(\frac{m_R}{\beta_o}\right) + \ell n\left[(1-\gamma_o)^2 f_y - \gamma_o{}^2 f_k\right] =$$

$$\left[\frac{\theta_{ext}(x_c)}{kT}\right] + \frac{\beta_o}{kT}\left\{\frac{\gamma_o(1-\gamma_o)\left[(1-\gamma_o) f_y + \gamma_o f_k\right]}{(1-\gamma_o)^2 f_y - \gamma_o{}^2 f_k}\right\}, \tag{45a}$$

$$\frac{E_c}{kT} = \ell n\left(\frac{m_R}{\beta_o}\right) + \ell n\left[(1-\gamma_o)^2 f_y - \gamma_o{}^2 f_k\right]. \tag{45b}$$

Equation (45a) is a transcendental equation which can determine x_c. It has a weak dependence on E_c, due to the nonlinear space-charge functions, f_y and f_k. For a given value of x_c, Eq. (45b) then gives the barrier height E_c. The true roots of Eqs. (45a) and (45b), $E_c{}^*$ and $x_c{}^*$, can now be easily determined using the following procedure.

Begin with $\theta_{ext}(x)$, and determine the intrinsic barrier maximum, in the absence of any space-charge effects:

$$\max\ [\theta_{ext}(x)] \equiv E_c^0. \tag{46}$$

Using E_c^0 as an initial value, $f_y(E_c^0)$ and $f_k(E_c^0)$ are evaluated using Eqs. (39a)-(39b). Equation (45a) then determines the x_c position based on the properties of the original $\theta_{ext}(x)$ function and its first derivative (through the β_o term). This x_c value can then be substituted into Eq. (45b), along with the $f_y(E_c^0)$ and $f_k(E_c^0)$ values, to determine a modified barrier height value, E_c^1. The E_c^1 can now be used in place of E_c^0, and the process repeated. After a few iterations, this procedure converges to the values E_c^* and x_c^*, which are the real roots of Eqs. (45a) and (45b).

E. RELATIONSHIP OF BARRIER HEIGHT TO EMISSION CURRENT

Equations (39a)-(39b) and (45a)-(45b) represent one major result of this report. The values E_c^* and x_c^* for the barrier height and position are determined using the particular effective potential approximation which is contained in the f_y and f_k terms. To change the effective potential only alters the f_y and f_k integrals, the rest of the procedure remaining the same. In this manner, the original nonlinear Poisson's equation is reduced to root-finding. The collected current density, which is determined by the total amount of electrons which can surmount the barrier, is then given by:

$$J_{net} = A_o T^2 \exp\ [-(E_c^* + \phi_e)]/kT, \tag{47}$$

where A_{oo} is Richardson's constant, and ϕ_e is the emitter work function. From E_c^* and Eq. (47), approximate current-voltage (I-V) and current-temperature (I-T) characteristics can be constructed.

IV. THE UNIFORM WORK FUNCTION CASE

A. THE SPACE-CHARGE AND TEMPERATURE-LIMITED CURRENTS

In this section, the effective potential method for generating approximate I-V and I-T curves is applied to the uniform work function emitter, with both Schottky barrier lowering and space-charge effects included. We first define a Richardson's Current J_R by:

$$J_R = A_o\, T^2 \exp\,[-\phi_e/kT], \tag{48}$$

and we also define a Child's Law Current J_C by:

$$J_C = \frac{4\,\epsilon_o}{9\,d^2}\left(\frac{2e}{m}\right)^{1/2}(\theta_E/e)^{3/2} \equiv \frac{K\,(\theta_E/e)^{3/2}}{d^2} \tag{49}$$

where K is 2.33525×10^{-6} amps/volt$^{3/2}$, and where θ_E is:

$$\theta_E = e\,V_A + \phi_e - \phi_c, \tag{50}$$

V_A is the applied external potential, and ϕ_e and ϕ_c are the emitter and collector work functions. The J_R and J_C currents help organize the parameters in the effective potential approximation to more clearly exhibit the transition from space-charge limited (SCL) to temperature-limited (TL) behaviors.

The effective potential method begins with specifying the potential energy function for an individual electron in the limit of no net current, $\theta_{ext}(x)$. For a uniform applied field with a near-cathode image-force potential, $\theta_{ext}(x)$ can be written as:

$$\theta_{ext}(x) = -\,(x/d)\,\theta_E - e^2/[16\,\pi\,\epsilon_o(x+x_a)], \tag{51}$$

where x_a is an "added distance" which prevents the image force potential from being singular at the cathode (x=0). The boundary condition at the cathode sets the value of x_a via:

$$e^2/[16\,\pi\varepsilon_o\,x_a] = +\phi_e. \tag{52}$$

For a work function of ϕ_e = 2 eV, $x_a \approx$ 1.8 Å. An additional image force for the near-collector region can also be included in Eq. (51) for increased accuracy at near-retarding field voltages.

The effective potential method presents two algebraic equations, Eqs. (42a)-(42b) or Eqs. (45a)-(45b), whose roots, E_c and x_c, represent the approximate barrier height and barrier position, in the presence of space-charge effects. The critical parameters from the external applied potential, $\theta_{ext}(x)$, are its value at x_c and its derivative at x_c. For the potential of Eq. (51), the derivative term is:

$$\beta_o \equiv -d\,\frac{d\,\theta_{ext}}{dx}\Big|_{x_c} = \theta_E - \frac{e^2\,d}{16\,\pi\varepsilon_o\,(x_c + x_a)^2}\,. \tag{53}$$

The nonlinear coupling, i.e., how the space-charge affects the current between the cathode and the anode, was expressed in terms of two additional functions, labelled f_y and f_k, which both depend on the barrier height E_c, but not the barrier distance.

The function f_k is only a function of the combined parameter $\Lambda = (E_c + \phi_e)/kT$, and as we show later, the essential transition from SCL to TL operation does not critically depend on f_k. The function f_k turns out to be more critical in the very low field regime, where there is another transition from SCL operation to what we will call almost-retarding-field (ARF) operation. This ARF regime is characterized by significant deviations from a Child's Law type behavior.

The function f_y is only a function of the combined parameter $\Lambda = (E_c + \theta_E)/kT$. For applied voltages greater than a few volts (i.e., outside ARF, but allowing either SCL or TL regimes), one will automatically be in the large Λ limit of f_y. As shown in the appendix [Eq. (A-14)], for large Λ:

$$f_y(\Lambda) \approx \frac{9}{8R} - \frac{3\,C_o}{2\,R^{3/2}} + [\text{Order } (R^{-3})], \tag{54}$$

where $R^2 \equiv (\pi\Lambda/4)$.

In Eq. (54), the parameter C_o is an integration constant which depends on the details of the entire inter-electrode potential. The effective potential method, by using an approximate function for the inter-electrode potential, can result in an error in the determination of C_o. As such, Eq. (54) may only be accurate to the first term. However, we show next that the leading term in f_y:

$$f_y \approx 9/8R = \frac{9}{8}\left[\frac{\pi\,(\theta_E + E_c)}{4kT}\right]^{-1/2}, \tag{55}$$

is sufficient to generate a SCL to TL transition.

The transition from SCL to TL behavior can be shown most easily using Eqs. (42a)-(42b). Both those equations are expressed in terms of a scaled distance, $\gamma_o = x_c/d$, where x_c is the distance to the barrier maximum, and d is the anode-cathode separation. For conditions that are not ARF, γ_o is expected to be small. Neglecting terms of order γ_o^2 in Eq. (42a) gives:

$$\beta_o \approx m_o\,(1 - 2\,\gamma_o)\,f_y, \tag{56a}$$

$$m_o = m_R \exp(-E_c/kT). \tag{56b}$$

The parameter m_R [see Eq. (43b)] can be expressed in terms of the currents J_R and J_C as follows:

$$m_R = \frac{8}{9} \frac{J_R}{J_C} \left(\frac{\pi \theta_E^3}{4 kT}\right)^{1/2} \cdot \cdot \tag{57}$$

Substituting Eqs. (53), (55), (56b), and (57) into Eq. (56a), and neglecting x_a as small compared to x_c, then gives:

$$\theta_E - \frac{e^2 d}{16 \pi \varepsilon_o x_c^2} \approx$$

$$\theta_E \frac{J_R}{J_C} \left(\frac{\theta_E}{\theta_E + E_c}\right)^{1/2} \left(1 - \frac{2 x_c}{d}\right) \exp\left[-E_c/kT\right]. \tag{58}$$

The near unity terms in Eq. (58) can be further approximated by unity for examining the SCL to TL transition, giving:

$$J_R \exp\left(-E_c/kT\right) \equiv J_{net} \approx \tag{59}$$

$$\frac{J_C}{\theta_E}\left(\theta_E - \frac{e^2 d}{16 \pi \varepsilon_o x_c^2}\right).$$

Equation (59), by itself, embodies a SCL-to-TL transition. When the barrier position wanders on the order of 1-μm away from the cathode, for d ≈ 1-cm, the x_c correction term in Eq. (59) is small (≈ 3.6 eV). Under these conditions, Eq. (59) shows that $J_{net} \approx J_C$, which is SCL operation. For higher applied fields, the barrier maximum moves closer to the cathode, and the x_c correction term in Eq. (59) then becomes a significant fraction of θ_E. The net resulting current is then less than Child's Law would have predicted at those applied voltages, and one is in TL operation.

Examining the other equation involving x_c and E_c [Eq. (42b)], it has a term in it which is solely a function of the external applied potential, $\theta_{ext}(x)$. For the $\theta_{ext}(x)$ function here [Eq. (51)], the terms in Eq. (42b) can be combined as follows:

$$\theta_{ext}(x_c) + \gamma_o \beta_o \approx -2e^2/(16 \pi \varepsilon_o x_c), \tag{60}$$

which gives for Eq. (42b):

$$E_c = - [2e^2/(16 \pi \varepsilon_o x_c)] + m_R (x_c/d)^2 f_k \exp(-E_c/kT). \quad (61)$$

The contribution to the net barrier height E_c in Eq. (61) from Eq. (60) is necessarily negative, since it corresponds to Schottky barrier lowering. The contribution to E_c involving f_k is necessarily positive, and corresponds to raising of the electron barrier, due to space-charge effects. Similar to how Eq. (59) changes with x_c value, one sees that large x_c values give a large space-charge term and a small Schottky barrier term. This makes E_c tend to be positive giving rise to SCL emission. Conversely, small x_c values are associated with a small space-charge term and a large Schottky barrier term, corresponding to TL emission.

For SCL emission, E_c can be positive. Equation (61) then shows that the f_k-term has a central role in allowing E_c to be positive. In contrast, Eq. (59), and its "parent" equation, Eq. (42a), have only a weak or no dependence on f_k. Thus, when Eq. (59) reduces to $J_{net} \approx J_C$ in the SCL regime, it means that Eq. (59) is practically determining E_c by itself, since J_{net} contains E_c. With E_c almost exactly specified in SCL emission by Eq. (60), the role of Eq. (61) and thus the role of the f_k-function in SCL-emission is then changed into primarily determining barrier position.

For TL emission, where Eq. (61) does help determine E_c, the effect of the f_k-function term is again only a small perturbation because x_c is then small. Thus, the f_k function is never critically involved in the emission current determination, anywhere from the SCL emission regime through to TL emission. This verifies what was mentioned earlier, that value of f_k is not essential to generate an SCL-to-TL transition.

We thus have shown that it is the f_y function which critically determines the emission current, while f_k primarily affects the final determination of barrier position. We note that this separation of roles derives from the algebraic structure of Eqs. (42a)-(42b). It is this same algebraic structure of these equations that gives rise to the SCL-to-TL transition, rather than

the SCL-to-TL transition being embodied within the explicit functional form of the f_y and f_k functions. The same function for f_y [Eq. (55)] carries over into both SCL and TL regimes. And in both regimes, f_k does not significantly affect the emission current. These are some of the reasons why the effective potential method, as outlined in this report, can give good approximations to cathode I-V and I-T curves, using just a simple power-law approximation for the nonlinear part of the original Poisson's equation (from where f_y and f_k derive).

B. A MODIFICATION TO SCHOTTKY BARRIER LOWERING

The SCL emission current was found to approximately be given by $J_{net} \approx J_C$ (Child's Law Current). We next derive an expression for J_{net} in TL emission limit.

For the TL emission limit, it is convenient to rewrite Eq. (59) as:

$$\frac{e^2 d}{16 \pi \varepsilon_o \theta_E} = x_c^2 \left(1 - \frac{J_{net}}{J_C}\right). \tag{62}$$

Substituting this into Eq. (61) and ignoring the f_k term as being small for TL operation, then gives:

$$E_c \approx - \left[\frac{e^2 \theta_E}{4 \pi \varepsilon_o d} \left(1 - \frac{J_{net}}{J_C}\right)\right]^{1/2}, \tag{63}$$

for the Schottky barrier lowering in TL emission, where $J_{net} < J_C$. Equation (63) agrees with the standard value of the Schottky barrier lowering, with a new correction term of order (J_{net}/J_C). This new correction term makes the collected current less, due to a persistence of some residual space-charge effects, at high applied fields.

The approximate solution to the effective potential method equations thus shows that $J_{net} \approx J_C$ (Child's Law) is valid over much of the SCL-regime, but a modification to Schottky barrier lowering is required for high-voltages, due to residual space-charge effects [Eq. (63)]. The Child's Law limit is valid for barrier heights $E_c > 0$, and E_c vanishes at $J_{net} = J_R$. The two solutions

for low and high fields thus join together. In addition, the derivative also can be shown to be continuous. This property allows the essential aspects of a SCL-to-TL transition to be summarized in a single equation:

$$J_{net} \approx \begin{cases} J_C, \ (J_R > J_C) & (64a) \\ J_R, \ (J_R = J_C) & (64b) \\ J_R \exp \frac{+1}{kT} \left[\frac{e^2\theta_E}{4\pi\varepsilon_o d}\left(1 - \frac{J_{net}}{J_C}\right)\right]^{1/2}, \ (J_R < J_C) & (64c) \end{cases}$$

to approximate the emission current with both Schottky barrier lowering and space-charge effects included. Equation (64) is Child's Law with a modified Schottky barrier lowering.

In Fig. 2, we examine how the approximate answer of Eq. (64) compares with using the full transformation of Eqs. (42a)-(42b). The comparison of Fig. 2 was generated using a work function of 2eV, 1050°C temperature, and an anode-cathode distance of 0.0256 cm.

Figure 2 shows that from SCL-emission near the Richardson current, up through the entire TL-region, the approximate solution, Eq. (64), is practically indistinguishable from the effective potential method calculation using the full equations of Eqs. (42a)-(42b). The full equations do show a difference in the deep SCL-region due to deviations from Child's Law in that regime.

Equation (64) thus represents a major result of the effective potential method. This method has analytically calculated the approximate emission current expected with both Schottky-barrier lowering and space-charge effects included, summarizing the difficult SCL-to-TL transition in terms of a single modified Schottky-barrier lowering term.

In the next sections, we show how this effective potential method compares to other results for I-V curves.

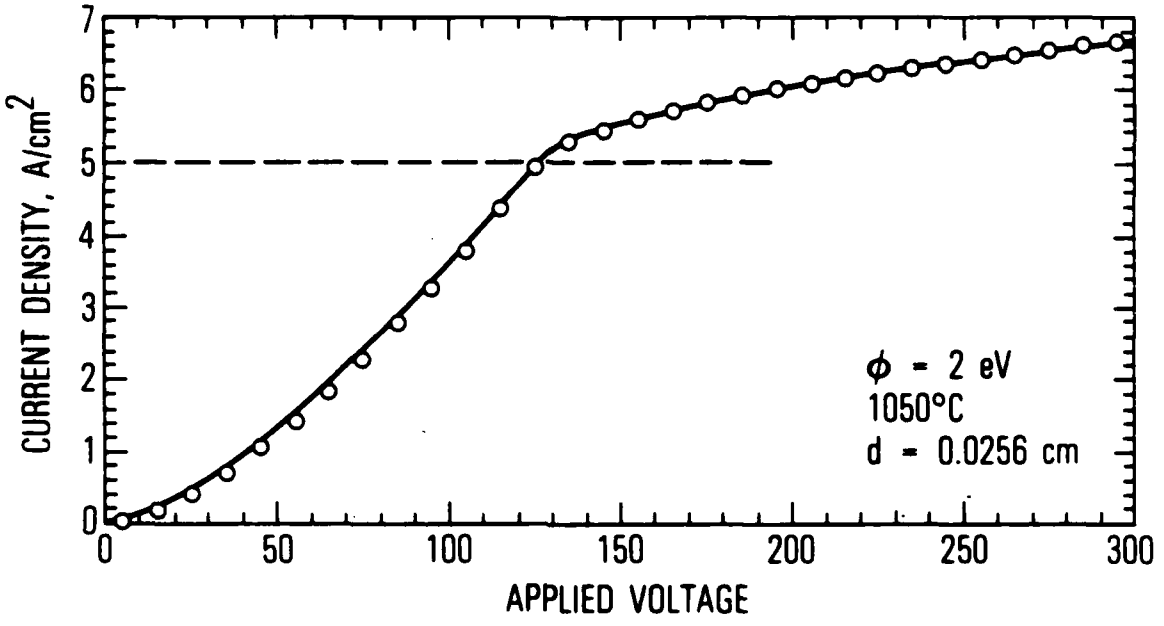

Fig. 2: Predictions of the "effective potential" approximation. A closed-form equation which approximates the current density vs. voltage [open circles, Eq. (64) in text] is compared with the more complete transformation equations of the effective potential method (solid line). The closed form approximation is seen to be very accurate in describing the predictions of the present method in the temperature-limited (TL) regime. The deviations at low voltages are due to Child's Law being inaccurate in the deep space-charge limited (SCL) regime. A dashed line marks the Richardson current, which is the SCL to TL transition point. The calculations were done using a work function of ϕ = 2.0 eV, a temperature of 1050°C, and an anode-cathode spacing of 0.0256 cm for all figures.

C. COMPARISON TO SCHOTTKY AND CHILD'S LAW CURRENTS

In this section, approximate cathode I-V curves, generated by the effective potential method, are compared to Child's Law and the Schottky barrier lowering currents. Here, the full transformations [Eqs. (42a)-(42b)] were used for E_c and x_c. Also, Eq. (A-4), in the appendix, is used for the f_k function, and the large argument form [Eq. (55)] is used for f_y. The f_y function critically determines the emission current, while f_k primarily affects the final determination of barrier position.

Figure 3 shows the results of a comparison of the effective potential method to Child's Law and the standard form of Schottky-barrier lowering. Noteworthy is the fact that the effective-potential method predicts a net current density that is significantly below the pure Schottky-line. As noted earlier, this corresponds to residual space-charge effects even in the high voltage limit. And, as was shown in Fig. 2, Eq. (64) is an excellent approximation to the results in this regime.

In Fig. 4, we plot the same results as Fig. 3, using logarithmic axes. This plot emphasizes the structure of the I-V curve in deep SCL-emission. Child's Law is a straight line of 3/2-slope on this graph, and Fig. 4 shows that significant deviations from Child's Law occur in the very low voltage regime. This effect is due to the Maxwellian distribution of electrons being explicitly considered here, with some high energy electrons always capable of surmounting the energy barrier.

In Fig. 5, we plot the predicted barrier position. As noted earlier, the effective potential method is expected to give greater inaccuracies in barrier position determination, while maintaining a small error in net emission current determination. The barrier position inaccuracies should be greatest in the SCL region, with less of an error in the transition and TL regions. Figure 5 also shows a dramatic transition point, where large changes in the barrier position occur over very small changes in applied voltage. This sharp change reflects an inherent transition in the system from SCL-to-TL emission, near the Richardson current point.

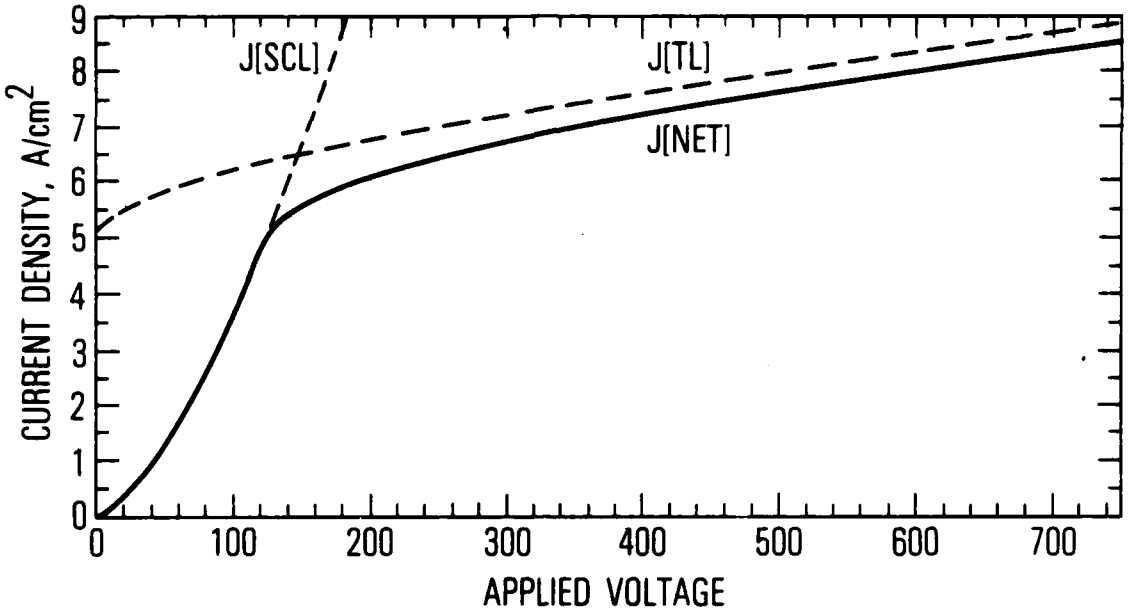

Fig. 3: Comparison of the present method (J[NET]) to the Schottky (J[TL]) and Child Law (J[SCL]) limits. The net current at low voltages is larger than predicted on the basis of Child's Law alone. At high voltages, the net current also remains a fraction below the Schottky line, due to the persistence of space-charge effects, deep into the temperature-limited regime.

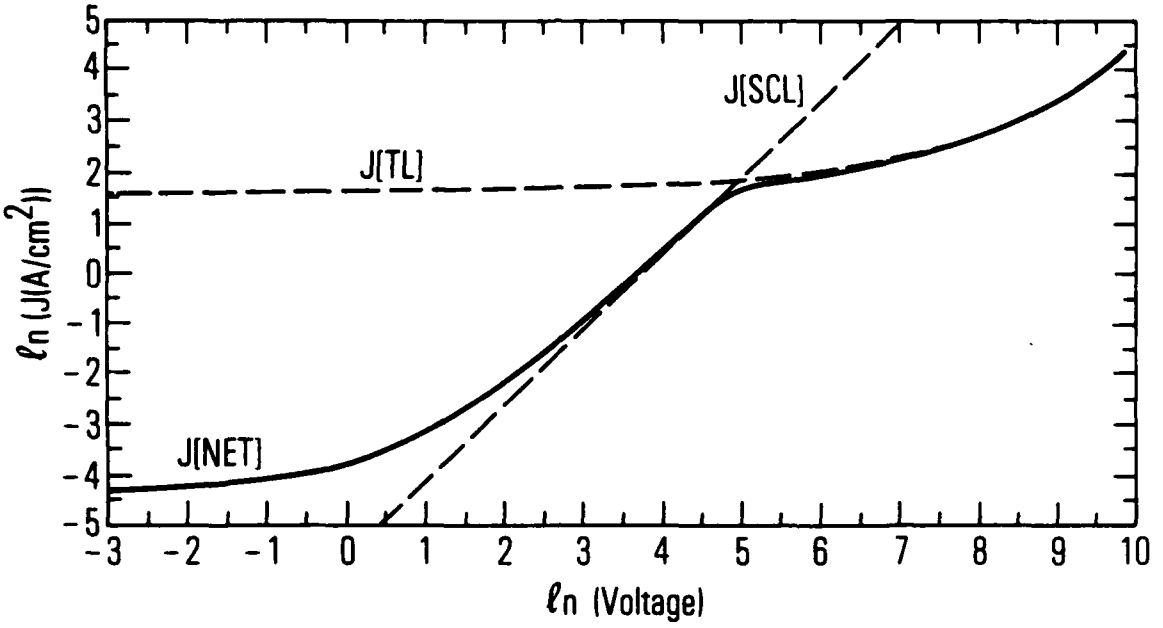

Fig. 4: A plot of current density vs. voltage on logarithmic axes. In this plot, Child's Law is a line of slope 3/2. The present method predicts significant deviations from Child's Law at low voltages due to the Maxwellian distribution in energy of the emitted electrons being taken into account here.

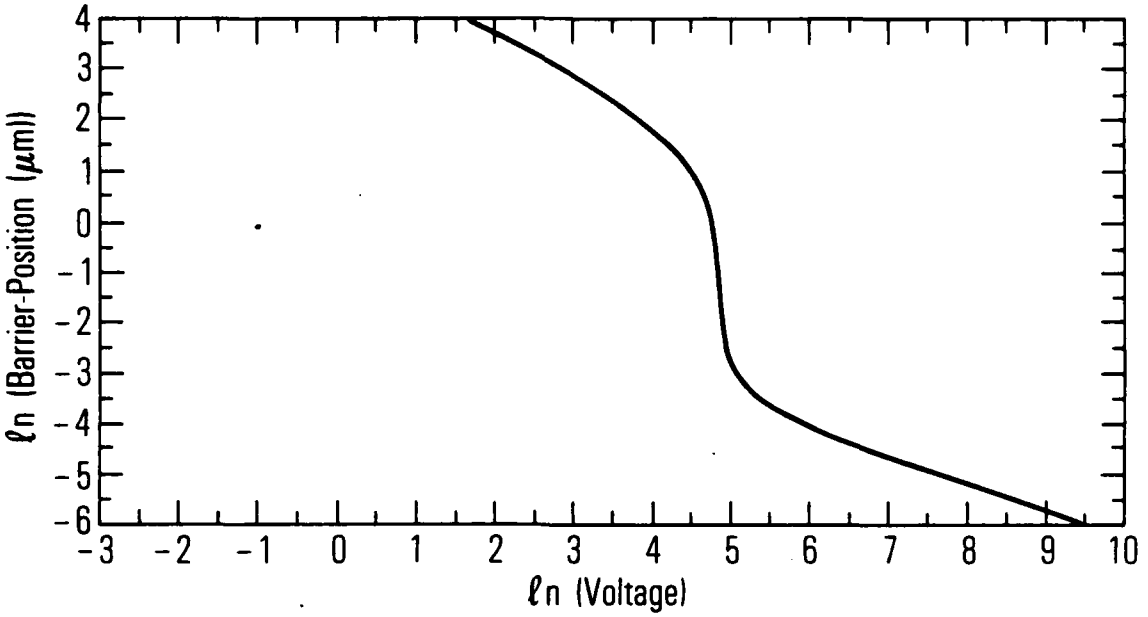

Fig. 5: Predictions for barrier position vs. voltage. There is a large change in barrier position within a narrow range of voltage. This point corresponds to the transition between SCL and TL emission.

D. COMPARISON WITH OTHER APPROXIMATE METHODS

In this section, the approximate cathode I-V curves, generated by the effective potential method, are compared to two prior methods, one by Scott,[11] and which Hasker[12] has analytically approximated, one by Longo.[10]

Historically, Langmuir[4] modified the simple $V^{3/2}$ power law of Child[3] for emission current density. As a function of applied voltage, the Langmuir solution begins in the almost-retarding-field (ARF) regime with significant deviations from Child's law, followed by a range where Child's law is approximately valid, then it abruptly bends over to the Richardson current value, first reaching the Richardson current value at some critical voltage, V_L.

Schottky[6] published his modification to the Richardson current the same year, but adding Schottky barrier lowering to the Langmuir solution has been slow to develop. Scott[11] attacked the problem by assuming the Langmuir solution is entirely valid for voltages less than V_L, even in the presence of Schottky barrier lowering. For voltages greater than V_L, he replaces the applied field in the Schottky barrier lowering effect, with an "effective field" derived from the local Langmuir potential. Using this technique, he circumvents the inhomogeneous part of the nonlinear Poisson's equation. The joining of solutions at V_L was noted by Scott to give rise to a "kink" in the solution, where the current vs. voltage goes from horizontal (zero slope) to a substantial slope just after V_L.

Longo's method[10] is almost semi-empirical. He finds that some data on actual cathodes seem to fit the equation:

$$(1/J_{net}) = (1/J_C) + (1/J[TL]), \tag{65}$$

where J[TL] is the standard temperature-limited value for current density with Schottky barrier lowering included, and where J_C is Child's law. The appeal of Longo's equation is its simplicity.

In some sense, the present work is similar to both Scott and Longo. Like Scott, we circumvent dealing with the full inhomogeneous nonlinear Poisson's

equation, making both Scott and this solution different approximate answers to the same problem. Scott uses the Langmuir equation for the nonlinearity part, "patching-in" Schottky barrier lowering using an effective field. Here, we dealt explicitly with the inhomogeneous Poisson's equation which describes Schottky barrier lowering, and we "patched-in" the nonlinearity by using an effective potential.

However, like Longo, we sought to preserve as much simplicity as possible in our approximate solution, by keeping our solution close to the domain of elementary functions. The hope, implicit in Longo's work, is to have a single equation describing cathode behavior from the space-charge limited (SCL) to the temperature-limited (TL) regime. That goal is realized, to a much greater degree of accuracy than Longo's equation, by Eq. (64) of this work.

Figure 6 plots the current vs. voltage, using logarithmic axes, for the same conditions as in Fig. 4: 1050°C, 2 eV work function, and an anode-cathode distance of 0.0256 cm. It compares the result of this work (solid line) to the prior work of both Scott and Longo (dotted lines).

At low voltages, *Longo's equation* asymptotically approaches Child's Law from below, with the other methods giving more current than Child's Law due to contributions from the high energy tail of thermally excited electrons in the emitter. The present work overestimates the current in this low-voltage ARF regime the most, mainly due to neglecting the explicit contribution of electrons which can form a trapped-cloud near the emitter surface. Scott's work uses Langmuir's solution at these lowest voltages, but even at eV values comparable to kT, this work is accurate to within a factor of two.

On the broad scale of Fig. 6, covering more than four decades in both voltage and current, Scott and this solution are similar. Longo's equation is low by a fair margin, except in the deep temperature-limited region.

The critical transition or knee region between SCL and TL operation is shown on an expanded scale in Fig. 7. In this transition region, the general shape predicted by both Scott and this work is similar. Scott gives a net emission current slightly higher by a few percent than this work, although an exact numerical calculation is needed to determine which method is relatively

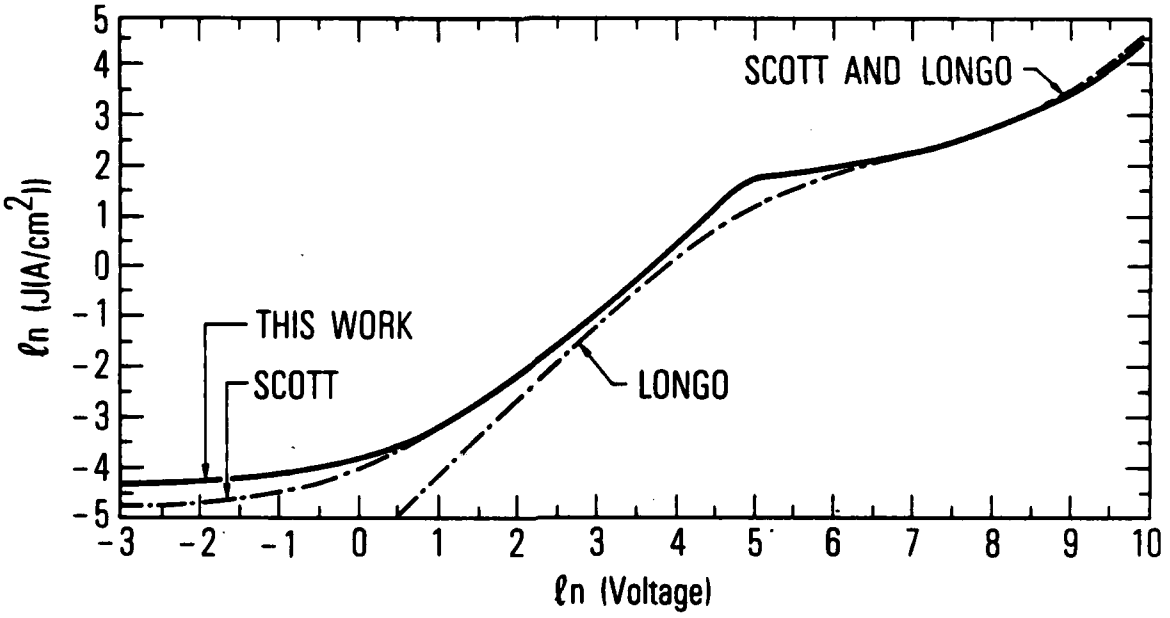

Fig. 6: Comparison of current density vs. voltage predictions among several methods. The approximate methods of this work, Scott, and Longo are compared over several orders of magnitude in both current and voltage. The Longo equation is low by a fair margain except in the deep temperature-limited region, with the other methods giving similar results on this scale.

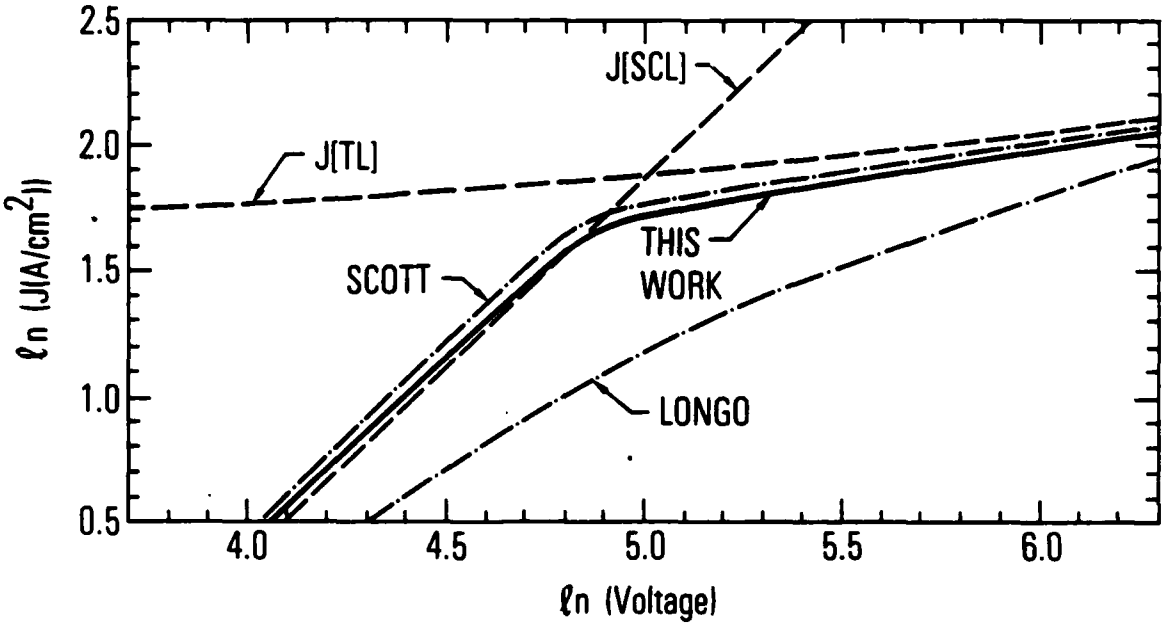

Fig. 7: Comparison as in Fig. 6, on an expanded scale, emphasizing the "knee" or transition region from SCL to TL operation. Child's Law and the Schottky barrier lowering limit are also shown for comparison. This work predicts values that are a few percent lower in the knee region than the Scott approximation.

more accurate here. Both break away from Child's Law, giving more SCL current, with this work being more gradual than Scott. In the TL region, the Scott result seems to approach the Schottky line faster than this work.

In Fig. 8, we plot the relative error among the several methods. This work was chosen as the 0% baseline. The vertical axis is percent error in emission current, spanning only 25% net difference, while the horizontal axis spans four orders of magnitude in voltage.

Figure 8 clearly shows that this work remains bounded away from the pure temperature-limited line (J[TL]) of Schottky barrier lowering. [Equation (64] is also plotted on Fig. 8. It is a one-line approximation to this work, and it has the accuracy of Child's law in the SCL regime.

Examining the TL-region of the Scott solution and the Longo equation in Fig. 8 shows that they both approach the J[TL] line too quickly. This effect is due to both methods not taking into account the residual space-charge effects in the TL-region.

The comparison of methods in Figs. 6-8 supports the usefulness and overall accuracy of this new method. In addition, the closed-form analytic correction to Schottky barrier lowering Eq. (64) retains practically all of the essential features associated with knee-roundedness, and it can be used as a simple approximation to the TL-emission region for uniform work function emitters.

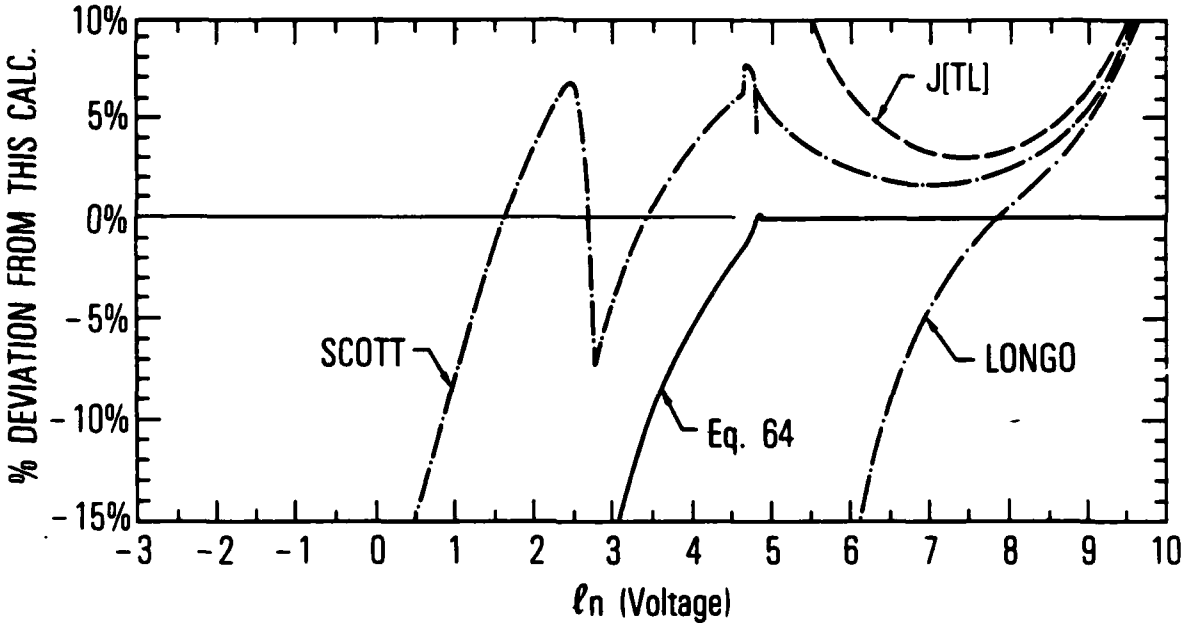

Fig. 8: Comparison of relative percent-error among the different methods. Both this work and Scott are similar although this work tends to be smoother. The closed-form approximation of Eq. (64), which is a new correction to Schottky barrier lowering, is also shown. Equation (64) has the accuracy of Child's Law in the SCL regime, and virtually the same accuracy as this work in the TL region. The high voltage region also shows that the Scott and Longo methods approach the usual Schottky barrier lowering current J[TL] too quickly.

V. CONCLUSIONS

In this work, we have developed a new technique for approximating the emission current from a planar thermionic emitter in a diode-type geometry. In general, this procedure reduced the nonlinear Poisson's equation to finding the roots of two algebraic equations. These two roots, labelled E_c and x_c, correspond to the net barrier height for electron emission, and net barrier distance from the cathode.

This method was then applied to the problem of a uniform work function surface with both Schottky barrier lowering and space-charge effects included. The equations for the roots E_c and x_c in this case were solved using root-finding routines, and the net emission current was compared to previously published approximations[10,11] for the uniform work function case. Scott's numerical method and this analytic one were found to quantitatively agree on cathode emission current to within ≈ 10% over a wide range of applied voltage.

In addition, the analytic formalism, although approximate, allowed us to derive a new closed form, representing a first correction to Schottky barrier lowering, due to space-charge effects being included. Physically, this new correction term, not included in any previous approximation, corresponds to a persistence of space-charge effects deep into the temperature-limited regime. This closed form specifies the roundedness of the knee-region between space-charge limited (SCL) and temperature-limited (TL) emission for the uniform work function case. It determines the SCL-to-TL transition point as being the Richardson's current. The closed form, approximating the emission current density for a uniform work function surface, was found to be:

$$J_{net} \approx J_C, \text{ for } J_C < J_R, \text{ and} \tag{66a}$$

$$J_{net} \approx J_R \exp + [\Delta\phi_o (1 - J_{net}/J_C)^{1/2}]/kT, \text{ for } J_C > J_R. \tag{66b}$$

In this equation, J_{net} is the total emission current density, J_R and J_C are the Richardson and Child Law current densities, and $\Delta\Phi_o$ is the usual value for Schottky barrier lowering. This simple approximation for J_{net} is also continuous at J_R, with a continuous first derivitive.

REFERENCES

1. O. W. Richardson, Phil. Mag. 23, 594 (1912).

2. S. Dushman, Phys. Rev. 21, 623 (1923).

3. C. D. Child, Phys. Rev. 32, 498 (1911).

4. I. Langmuir, Phys. Rev. 21, 419 (1923).

5. W. Schottky, Z. Physik 14, 63 (1923).

6. W. B. Nottingham, "Thermionic Emission", Report 321, MIT Research Laboratory of Electronics (10 Dec. 1956).

7. A. Van der Zeil, Philips Res. Rep. 1, 97 (1946).

8. C. R. Crowell, J. Appl. Phys. 26, 1353 (1955).

9. E. S. Rittner, J. Appl. Phys. 31, 1065 (1960).

10. R. T. Longo, IEEE Trans. Electron Devices, 152 (1980).

11. J. B. Scott, J. Appl. Phys. 52, 4406 (1981).

12. J. Hasker, Applic. Surf. Sci. 16, 220 (1983).

13. I. S. Gradshteyn and I. M Rhyzik, "Tables of Integrals, Series, and Products," Academic Press (1965), p. 620.

14. M. Abramowitz and I. A. Stegun, "Handbook of Mathematical Functions," National Bureau of Standards (1972), p. 298.

APPENDIX: THE f_y AND f_k FUNCTIONS

In this appendix, we solve the two integrals, Eqs. (39a) and (39b), which determine the nonlinear f_y and f_k terms.

A. THE f_k- FUNCTION

The integral representing the f_k- term is:

$$f_k(\Lambda) = \int_{u=-1}^{0} (1 + u)\, du \, \frac{(4/\pi)^{1/2}}{[\Lambda u^2]^{1/2} + [\Lambda u^2 + (4/\pi)]^{1/2}}. \tag{A-1}$$

Defining:

$$R^2 = \pi\Lambda/4, \tag{A-2}$$

The f_k-function can then be written as:

$$f_k(\Lambda) = \frac{1}{R} \int_{r=0}^{R} (1 - \frac{r}{R})\, dr/[(r^2 + 1)^{1/2} + r]. \tag{A-3}$$

These integrals can be done exactly, resulting in:

$$f_k = \frac{1}{2R} \ln [R + (R^2 + 1)^{1/2}] - \frac{(3R^2 - 4R)}{6(R^3 - 2) + 6(R^2 - 2)(R^2 + 1)^{1/2}} \tag{A-4}$$

for the f_k function.

B. THE f_y-FUNCTION

The integral representing the f_y-term is:

$$f_y(\Lambda) = \int_{w=0}^{1} (1 - w)\, dw \, \frac{(4/\pi)^{1/2}}{(\Lambda w^{4/3})^{1/2} + [\Lambda w^{4/3} + (4/\pi)]^{1/2}}. \tag{A-5}$$

Using the substitution:

$$r^2 = (\pi\Lambda/4)\, w^{4/3} \equiv R^2 w^{4/3}, \tag{A-6}$$

the f_y function can then be written as:

$$f_y(\Lambda) = \frac{3}{2R^{3/2}} \int_{r=0}^{R} \left[1-\left(\frac{r}{R}\right)^{3/2}\right] r^{1/2}\, dr/\left[\left(r^2+1\right)^{1/2} + r\right]. \tag{A-7}$$

The term:

$$E(R) \equiv \int_{r=0}^{R} \frac{r^{1/2} dr}{r + [r^2+1]^{1/2}} \tag{A-8}$$

is an elliptical integral, the other term being an elementary function.

Since $R^2 \propto (eV_A/kT)$, where V_A is the applied accelerating voltage, one is generally interested in the large R limit for the f_y function. A large R expansion for the elliptical integral, E(R), is:

$$E(R) \propto R^{1/2} - C_o + (12R^{3/2})^{-1} + [\text{Order } (R^{-7/2})] \tag{A-9}$$

where C_o is an integration constant.

The particular value of C_o, specified by choosing the lower limit of Eq. (A-8) to be r=0, is:

$$C_o \propto 0.677771, \tag{A-10}$$

determined numerically. It is important to note that C_o is a parameter in the large R expansion of E(R) which is sensitive to the behavior at small R. Thus C_o is sensitive to details of the effective potential which was chosen.

The other integral appearing in the f_y function:

$$F(R) = \int_{r=0}^{R} \frac{r^2 dr}{r + (r^2 + 1)^{1/2}} \qquad \text{(A-11)}$$

can be done exactly using the substitution $r = \sinh(z)$. The large R expansion for F(R) is:

$$F(R) = R^2/4 - [\ln(R) + C_1\ ]/8 - (32\ R^2)^{-1} + [\text{Order}\ (R^{-4})]. \qquad \text{(A-12)}$$

C_1 is another constant of integration in the large R expansion which is sensitive to the details of the effective potential, similar to C_o. The particular value of C_1 for Eq. (A-10) is:

$$C_1 = (\ln 2 - 1/4) \approx 0.443147. \qquad \text{(A-13)}$$

This gives the following large R expansion for the function f_y:

$$f_y \approx \frac{9}{8R} - \frac{3\ C_o}{2\ R^{3/2}} + \frac{[3\ln(R) + 3C_1 + 2]}{16\ R^3} - [\text{Order}\ (R^{-5})], \qquad \text{(A-14)}$$

where:

$$R^2 = (\pi\Lambda/4) \qquad \text{(A-15)}$$

The important conclusion for the f_y function is that in the region of interest (large R), f_y has an expansion whose leading term is (9/8R). Also, via C_o, it has a first correction term whose magnitude depends on the details of the potential between the electrodes, from the collector all the way back to the near cathode region.

LABORATORY OPERATIONS

The Laboratory Operations of The Aerospace Corporation is conducting experimental and theoretical investigations necessary for the evaluation and application of scientific advances to new military space systems. Versatility and flexibility have been developed to a high degree by the laboratory personnel in dealing with the many problems encountered in the nation's rapidly developing space systems. Expertise in the latest scientific developments is vital to the accomplishment of tasks related to these problems. The laboratories that contribute to this research are:

Aerophysics Laboratory: Launch vehicle and reentry fluid mechanics, heat transfer and flight dynamics; chemical and electric propulsion, propellant chemistry, environmental hazards, trace detection; spacecraft structural mechanics, contamination, thermal and structural control; high temperature thermomechanics, gas kinetics and radiation; cw and pulsed laser development including chemical kinetics, spectroscopy, optical resonators, beam control, atmospheric propagation, laser effects and countermeasures.

Chemistry and Physics Laboratory: Atmospheric chemical reactions, atmospheric optics, light scattering, state-specific chemical reactions and radiation transport in rocket plumes, applied laser spectroscopy, laser chemistry, laser optoelectronics, solar cell physics, battery electrochemistry, space vacuum and radiation effects on materials, lubrication and surface phenomena, thermionic emission, photosensitive materials and detectors, atomic frequency standards, and environmental chemistry.

Computer Science Laboratory: Program verification, program translation, performance-sensitive system design, distributed architectures for spaceborne computers, fault-tolerant computer systems, artificial intelligence and microelectronics applications.

Electronics Research Laboratory: Microelectronics, GaAs low noise and power devices, semiconductor lasers, electromagnetic and optical propagation phenomena, quantum electronics, laser communications, lidar, and electro-optics; communication sciences, applied electronics, semiconductor crystal and device physics, radiometric imaging; millimeter wave, microwave technology, and RF systems research.

Materials Sciences Laboratory: Development of new materials: metal matrix composites, polymers, and new forms of carbon; nondestructive evaluation, component failure analysis and reliability; fracture mechanics and stress corrosion; analysis and evaluation of materials at cryogenic and elevated temperatures as well as in space and enemy-induced environments.

Space Sciences Laboratory: Magnetospheric, auroral and cosmic ray physics, wave-particle interactions, magnetospheric plasma waves; atmospheric and ionospheric physics, density and composition of the upper atmosphere, remote sensing using atmospheric radiation; solar physics, infrared astronomy, infrared signature analysis; effects of solar activity, magnetic storms and nuclear explosions on the earth's atmosphere, ionosphere and magnetosphere; effects of electromagnetic and particulate radiations on space systems; space instrumentation.

END

FILMED

10-85

DTIC